Nonlinear Dyn (2012) 69:743–753
DOI 10.1007/s11071-011-0301-2

ORIGINAL PAPER

Determining Lyapunov spectrum and Lyapunov dimension based on the Poincaré map in a vibro-impact system

Yuan Yue · Jianhua Xie · Xuejun Gao

Received: 18 August 2011 / Accepted: 8 December 2011 / Published online: 22 December 2011

Abstract We develop a method to compute the Lyapunov spectrum and Lyapunov dimension, which is effective for both symmetric and unsymmetric vibro-impact systems. The Poincaré section is chosen at the moment after impacting, and the six-dimensional Poincaré map is established. The time between two consecutive impacts is determined by the initial conditions and the impact condition, hence the Poincaré map is an implicit map. The Poincaré map is used to calculate all the Lyapunov exponents and the Lyapunov dimension. By numerical simulations, the attractors are represented in the projected Poincaré section, and the Lyapunov spectrum is obtained. The multi-degree-of-freedom vibro-impact system may exhibit complex quasi-periodic attractors, which can be characterized by the Lyapunov dimension.

Keywords Vibro-impact · Lyapunov exponents · Lyapunov dimension · Quasi-periodic attractor

Y. Yue (✉) · J. Xie
School of Mechanics and Engineering, Southwest Jiaotong University, Chengdu 610031, China
e-mail: peak8668@yahoo.com.cn

X. Gao
College of Environment and Civil Engineering, Chengdu University of Technology, Chengdu 610059, China

1 Introduction

The Lyapunov exponents measure the exponential rates of divergence or convergence of nearby orbits of an attractor in the state space, and are the most precise tool for identification of the character of motion in a dynamical system [1–4]. Wolf et al. [5] developed a method based on tracing the evolution of an initial sphere of small perturbation to a nominal trajectory, and Lyapunov exponents were obtained by the average rate of the logarithmic stretch of the ellipsoidal principal axes. Eckmann and Ruelle [6, 7] analyzed an algorithm for computing Lyapunov exponents from an experimental time series based on the QR methods. Brown and Bryant [8] examined the question of accurately determining the Lyapunov exponents of the dynamical system, and showed that it is advantageous to use local neighborhood-to-neighborhood mappings with higher-order Taylor series, rather than just local linear maps. Lu et al. [9] developed a method of Lyapunov vectors to computing Lyapunov exponents of continuous systems. A novel method for estimating Lyapunov exponents from a time series in the presence of additive noise corruption was presented in [10]. A new method was presented to calculate the Lyapunov spectrum of dynamical systems based on the time evolution of initially small disturbed copies ("clones") of the motion equations in [11]. Stefański and Kapitaniak [12] studied the estimation of the dominant Lyapunov exponent of non-smooth systems on the basis of maps

synchronization. It is also shown that for the non-smooth system, the calculation of Lyapunov exponents is not straightforward, and the required linearized equations have to be supplemented by certain transition conditions at the instants of discontinuities [13]. For systems with impact, several methods for the calculation of Lyapunov exponents have been proposed [14–18].

One intrinsic characteristic of attractors is their dimensions. The dimension of a limit set measures the amount of information necessary to specify points within it accurately. The dimensions of the attractor can give a lower bound on the number of state variables needed to describe the dynamics on the attractor, and can be used to quantify the complexity of an attractor. The Lyapunov spectrum is closely related to the fractal dimension of the associated attractor. In [19, 20], a relationship between the Lyapunov exponents of a map with a strange attractor and the dimension of the strange attractor was conjectured, and the Lyapunov dimension of an attractor was defined by Kaplan and Yorke. In [21], this conjecture was numerically tested with use of several different maps by Russell et al., and the result shows that the conjecture was verified to within the obtained accuracy. Some relations between dimensions and Lyapunov exponents were obtained rigorously by Ledrappier in [22].

In [23], a method of calculating all the Lyapunov exponents was proposed for a three-degree-of-freedom vibro-impact system with symmetric two-sided rigid constraints. The Poincaré map of the system has symmetry property, and can be expressed as the second iteration of another unsymmetric implicit map. Based on the QR method, this unsymmetric implicit map is used to calculate all the Lyapunov exponents. However, this method can only be applied for other vibro-impact systems *with symmetry*, because the unsymmetric implicit map exists only in the symmetric vibro-impact system.

In this paper, we develop a method based on the Poincaré map to compute the Lyapunov spectrum, which is effective for both symmetric and unsymmetric vibro-impact systems. In Sect. 2, the Poincaré section of the three degree-of-freedom vibro-impact system is chosen at the moment after impacting, and the six-dimensional Poincaré map is established. In Sect. 3, the Jacobi matrix of the Poincaré map is deduced analytically. In Sect. 4, the Jacobi matrix of the Poincaré map is used to calculate all the Lyapunov exponents and the Lyapunov dimension. In Sect. 5, by numerical simulations, the attractors are represented in the projected Poincaré section, and the Lyapunov spectrum is obtained. The multi-degree-of-freedom vibro-impact system may exhibit various complex quasi-periodic attractors, which can be classified by the Lyapunov dimension.

2 Mechanical model, Poincaré section and Poincaré map

A three degree-of-freedom system with symmetric rigid constraints is shown in Fig. 1. The system has three masses M_1, M_2, and M_3. M_2 and M_3 are connected to rigid planes via two linear springs K_2 and K_3, and two linear viscous dashpots C_2 and C_3, respectively. M_1 is connected to M_2 via linear spring K_1 and linear viscous dashpot C_1. The excitations on three masses are harmonic with amplitudes P_1, P_2, and P_3. For small forcing amplitudes, the system undergoes simple oscillations and behaves as a linear system. However, as the amplitudes increased, M_3 begins to collide with two stops of M_2, and the system becomes discontinuous and strongly non-linear. The impact is described by a coefficient of restitution R. It is assumed that the duration of impact is negligible compared to the period of the force, and the friction between M_3 and M_2 is negligible, also. C_1 and C_2 are assumed as proportional damping.

Between any two consecutive impacts, the non-dimensional differential equations of motion are given by

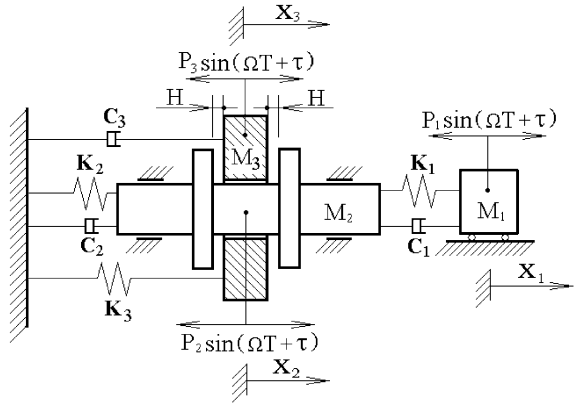

Fig. 1 A three-degree-of-freedom vibro-impact system

$$\left.\begin{aligned}
&u_{m1}\ddot{x}_1 + 2u_{c1}\zeta(\dot{x}_1 - \dot{x}_2) + u_{k1}(x_1 - x_2)\\
&\quad = u_{f1} f \sin(\omega t + \tau),\\
&u_{m2}\ddot{x}_2 + 2(u_{c1} + u_{c2})\zeta\dot{x}_2 - 2u_{c1}\zeta\dot{x}_1\\
&\qquad + (u_{k1} + u_{k2})x_2 - u_{k1}x_1\\
&\quad = u_{f2} f \sin(\omega t + \tau),\\
&u_{m3}\ddot{x}_3 + 2u_{c3}\zeta\dot{x}_3 + u_{k3}x_3\\
&\quad = u_{f3} f \sin(\omega t + \tau),
\end{aligned}\right\} \tag{1}$$

where the non-dimensional variables and parameters are

$$t = T\sqrt{\frac{K_3}{M_3}}, \quad \zeta = \frac{C_3}{2\sqrt{K_3 M_3}},$$

$$\omega = \Omega\sqrt{\frac{M_3}{K_3}}, \quad f = \frac{P_3}{P_0}, \quad u_{mi} = \frac{M_i}{M_3},$$

$$u_{ki} = \frac{K_i}{K_3}, \quad u_{ci} = \frac{C_i}{C_3}, \quad u_{fi} = \frac{P_i}{P_3}, \quad x_i = \frac{X_i K_3}{P_0},$$

$i = 1, 2, 3$, and $P_0 = |P_1| + |P_2| + |P_3|$. The phase angle τ is used only to make a suitable choice for the origin of time in the calculation.

When M_3 impacts the left and the right stops of M_2, the non-dimensional displacements of two masses satisfy $|x_2 - x_3| = h$, where $h = \frac{K_3 H}{P_0}$. After each impact, the velocities of M_2 and M_3 change according to the impact law:

$$\begin{aligned}
\dot{x}_{2+} &= m_1\dot{x}_{2-} + n_1\dot{x}_{3-},\\
\dot{x}_{3+} &= m_2\dot{x}_{2-} + n_2\dot{x}_{3-},
\end{aligned} \tag{2}$$

where

$$m_1 = \frac{u_{m2} - R}{1 + u_{m2}}, \quad n_1 = \frac{1 + R}{1 + u_{m2}},$$

$$m_2 = \frac{u_{m2}(1 + R)}{1 + u_{m2}}, \quad n_2 = \frac{1 - u_{m2}R}{1 + u_{m2}}.$$

In (1) and (2), a dot $(\cdot)$ denotes differentiation with respect to the non-dimensional time t. $\dot{x}_{i-}$ and $\dot{x}_{i+}$ represent the non-dimensional velocities of M_i before and after impacting, respectively.

The phase space of the vibro-impact system is

$$\begin{aligned}
&\mathbf{R}^6 \times \mathbf{S}^1\\
&\quad = \{x_1, y_1, x_2, y_2, x_3, y_3, t | (x_1, y_1, x_2, y_2, x_3, y_3)\\
&\qquad \in \mathbf{R}^6, t \in \mathbf{S}^1\},
\end{aligned} \tag{3}$$

where $\mathbf{S}^1$ is the $\frac{2\pi}{\omega}$ circle. The Poincaré section $\mathbf{\Pi}_0$ is chosen at the moment of impacting at the left stop, that is

$$\begin{aligned}
\mathbf{\Pi}_0 = \{&(x_1, y_1, x_2, y_2, x_3, y_3, t) \in \mathbf{R}^6 \times \mathbf{S}^1 | x_2 - x_3\\
&= h, y_i = \dot{x}_{i+}\},
\end{aligned} \tag{4}$$

and the section of impacting at the right stop can be expressed as

$$\begin{aligned}
\mathbf{\Pi}_1 = \{&(x_1, y_1, x_2, y_2, x_3, y_3, t) \in \mathbf{R}^6 \times \mathbf{S}^1 | x_2 - x_3\\
&= -h\}.
\end{aligned} \tag{5}$$

The Poincaré map $\mathbf{P}$ is a composition of following four sub-maps: (I) $\mathbf{P}_1$: The map from the instant after impacting at the left stop ($t = t_0$) to the instant before impacting at the right stop ($t = t_1$); (II) $\mathbf{P}_2$: The map of impacting at the right stop ($t = t_1$); (III) $\mathbf{P}_3$: The map from the instant after impacting at the right stop ($t = t_1$) to the instant before impacting at the left stop ($t = t_2$); (IV) $\mathbf{P}_4$: The map of impacting at the left stop ($t = t_2$). Then we establish the six-dimensional Poincaré map of the vibro-impact system as follows:

$$\mathbf{P} : \mathbf{\Pi}_0 \mapsto \mathbf{\Pi}_0, \quad \mathbf{P} = \mathbf{P}_4 \circ \mathbf{P}_3 \circ \mathbf{P}_2 \circ \mathbf{P}_1. \tag{6}$$

3 The Jacobi matrix of the Poincaré map

According to (6), the Jacobi matrix of the Poincaré map can be computed as

$$D\mathbf{P} = D\mathbf{P}_4 \circ D\mathbf{P}_3 \circ D\mathbf{P}_2 \circ D\mathbf{P}_1, \tag{7}$$

where $D\mathbf{P}_i$ is the linearized matrix of sub-maps $\mathbf{P}_i$.

At the moment of impact, the coordinates x_1, x_2, and y_1 do not change, and y_2, y_3 changes according to (2), then we obtain

$$D\mathbf{P}_2 = D\mathbf{P}_4 = \begin{bmatrix}
1 & 0 & 0 & 0 & 0 & 0\\
0 & 1 & 0 & 0 & 0 & 0\\
0 & 0 & 1 & 0 & 0 & 0\\
0 & 0 & 0 & m_1 & n_1 & 0\\
0 & 0 & 0 & m_2 & n_2 & 0\\
0 & 0 & 0 & 0 & 0 & 1
\end{bmatrix}. \tag{8}$$

Since $\mathbf{P}_1$ and $\mathbf{P}_3$ is two implicit maps, the corresponding Jacobi matrixes $D\mathbf{P}_1$ and $D\mathbf{P}_3$ are calculated according to implicit function theorem. Let $D\mathbf{P}_1 = [a_{ij}]_{6\times 6}$, the entries of the matrix $D\mathbf{P}_1$ are computed as follows. Subsequently, $D\mathbf{P}_3$ is obtained by the similar way.

The first and the second differential equations of (1) are coupling, and the eigenfrequencies can be solved as ω_1 and ω_2. Taking $\mathbf{\Psi}$ as the canonical model matrix,

and making the change of variables $[x_1, x_2]^{\mathbf{T}} = \mathbf{\Psi}\xi$, the first and the second equations of (1) become

$$\mathbf{I}\ddot{\xi} + \mathbf{C}\dot{\xi} + \mathbf{\Lambda}\xi = \bar{\mathbf{F}}\sin(\omega t + \tau), \tag{9}$$

where $\mathbf{C} = 2\zeta_p\mathbf{\Lambda} = diag[2\zeta_p\omega_1^2, 2\zeta_p\omega_2^2]$, $\bar{\mathbf{F}} = [\bar{f}_1, \bar{f}_2]^{\mathrm{T}} = \mathbf{\Psi}^{\mathrm{T}}P_k$, $P_k = [u_{f1}f, u_{f2}f]^{\mathrm{T}}$.

Let ψ_{ij} denotes the element of $\mathbf{\Psi}$, the general solution of (1) is given by

$$\left.\begin{aligned} x_1(t) &= \sum_{j=1}^{2}\psi_{1j}\big(e^{-\eta_j t}\big(a_j\cos(\omega_{dj}t) + b_j\sin(\omega_{dj}t)\big) \\ &\quad + A_j\sin(\omega t + \tau) + B_j\cos(\omega t + \tau)\big), \\ x_2(t) &= \sum_{j=1}^{2}\psi_{2j}\big(e^{-\eta_j t}\big(a_j\cos(\omega_{dj}t) + b_j\sin(\omega_{dj}t)\big) \\ &\quad + A_j\sin(\omega t + \tau) + B_j\cos(\omega t + \tau)\big), \\ x_3(t) &= e^{-\eta_3 t}\big(a_3\cos(\omega_{d3}t) + b_3\sin(\omega_{d3}t)\big) \\ &\quad + A_3\sin(\omega t + \tau) + B_3\cos(\omega t + \tau), \end{aligned}\right\} \tag{10}$$

where $\eta_j = \zeta_p\omega_j^2$, $\omega_{dj} = \sqrt{\omega_j^2 - \eta_j^2}$, $j = (1, 2)$, $\eta_3 = \zeta$, $\omega_{d3} = \sqrt{1 - \eta_3^2}$, and a_i and b_i are the integration constants, A_i and B_i are the amplitude constants:

$$\begin{aligned} A_j &= \frac{(\omega_j^2 - \omega^2)\bar{f}_j}{(2\eta_j\omega)^2 + (\omega_j^2 - \omega^2)^2}, \\ B_j &= \frac{-2\eta_j\omega\bar{f}_j}{(2\eta_j\omega)^2 + (\omega_j^2 - \omega^2)^2}, \quad (j = 1, 2) \end{aligned} \tag{11.1}$$

$$\begin{aligned} A_3 &= \frac{(u_{k3} - u_{m3}\omega^2)u_{f3}f}{(u_{k3} - u_{m3}\omega^2)^2 + (2u_{c3}\zeta\omega)^2}, \\ B_3 &= \frac{2u_{c3}\zeta\omega u_{f3}f}{(u_{k3} - u_{m3}\omega^2)^2 + (2u_{c3}\zeta\omega)^2}. \end{aligned} \tag{11.2}$$

Let the coordinates of the initial map point $\mathbf{x}^* \in \mathbf{\Pi}_0$ be $x_1^*, y_1^*, x_2^*, y_2^*, y_3^*, \tau^*$. Substituting $t = 0$ into (10), we obtain

$$\begin{aligned} x_i^* &= \psi_{i1}(a_1 + A_1\sin\tau^* + B_1\cos\tau^*) \\ &\quad + \psi_{i2}(a_2 + A_2\sin\tau^* + B_2\cos\tau^*), \\ &\quad i = 1, 2; \end{aligned} \tag{12.1}$$

and

$$\begin{aligned} y_i^* &= \dot{x}_i^* \\ &= \psi_{i1}(-\eta_1 a_1 + \omega_{d1}b_1 + A_1\omega\cos\tau^* - B_1\omega\sin\tau^*) \\ &\quad + \psi_{i2}(-\eta_2 a_2 + \omega_{d2}b_2 \\ &\quad + A_2\omega\cos\tau^* - B_2\omega\sin\tau^*) \quad i = 1, 2, \end{aligned} \tag{12.2}$$

$$x_3^* = a_3 + A_3\sin\tau^* + B_3\cos\tau^*, \tag{12.3}$$

Besides, since $x_2^* - x_3^* = h$ with $t = 0$, the following relation holds:

$$\begin{aligned} x_2^* - x_3^* &= \psi_{i1}(a_1 + A_1\sin\tau^* + B_1\cos\tau^*) \\ &\quad + \psi_{i2}(a_2 + A_2\sin\tau^* + B_2\cos\tau^*) \\ &\quad - (a_3 + A_3\sin\tau^* + B_3\cos\tau^*) \\ &= h. \end{aligned} \tag{12.4}$$

According to (12.1)–(12.4), the integration constants can be expressed as the function of the initial conditions:

$$a_1 = U_{a1}\sin\tau^* + V_{a1}\cos\tau^* + P_{a1}x_1^* + Q_{a1}x_2^*, \tag{13.1}$$

$$a_2 = U_{a2}\sin\tau^* + V_{a2}\cos\tau^* + P_{a2}x_1^* + Q_{a2}x_2^*, \tag{13.2}$$

$$a_3 = U_{a3}\sin\tau^* + V_{a3}\cos\tau^* + P_{a3}x_1^* + Q_{a3}x_2^* - h, \tag{13.3}$$

$$\begin{aligned} b_1 &= U_{b1}\sin\tau^* + V_{b1}\cos\tau^* + P_{b1}x_1^* + Q_{b1}x_2^* \\ &\quad + M_{b1}y_1^* + N_{b1}y_2^*, \end{aligned} \tag{13.4}$$

$$\begin{aligned} b_2 &= U_{b2}\sin\tau^* + V_{b2}\cos\tau^* + P_{b2}x_1^* + Q_{b2}x_2^* \\ &\quad + M_{b2}y_1^* + N_{b2}y_2^*, \end{aligned} \tag{13.5}$$

$$\begin{aligned} b_3 &= U_{b3}\sin\tau^* + V_{b3}\cos\tau^* + P_{b3}x_1^* + Q_{b3}x_2^* \\ &\quad + M_{b3}y_1^* - \frac{\eta_3}{\omega_{d3}}h. \end{aligned} \tag{13.6}$$

After the moment of impacting at the right stop, let the initial conditions be $x_1^*, y_1^*, x_2^*, y_2^*, y_3^*, \tau^*$, the integration constants a_1, a_2, and b_1, b_2 are the same expressions shown as (13.1), (13.2), and (13.4), (13.5). However, because the section of impacting is different, the expressions a_3 and b_3 are changed as

$$\begin{aligned} a_3 &= U_{a3}\sin\tau^* + V_{a3}\cos\tau^* + P_{a3}x_1^* \\ &\quad + Q_{a3}x_2^* + h, \end{aligned} \tag{14.1}$$

$$\begin{aligned} b_3 &= U_{b3}\sin\tau^* + V_{b3}\cos\tau^* + P_{b3}x_1^* + Q_{b3}x_2^* \\ &\quad + M_{b3}y_1^* + \frac{\eta_3}{\omega_{d3}}h. \end{aligned} \tag{14.2}$$

According to (12.1)–(12.4), the components of map $\mathbf{P}_1 = [\,P_{11}\ P_{12}\ P_{13}\ P_{14}\ P_{15}\ P_{16}\,]^{\mathrm{T}}$ are

$$\begin{aligned} P_{11} &= x_1(x_1^*, y_1^*, x_2^*, y_2^*, y_3^*, \tau^*) \\ &= \sum_{j=1}^{2}\psi_{1j}\big[e^{-\eta_j t}(a_j\cos\omega_{dj}t + b_j\sin\omega_{dj}t) \\ &\quad + A_j\sin(\omega t + \tau^*) + B_j\cos(\omega t + \tau^*)\big], \end{aligned} \tag{15.1}$$

$$\begin{aligned}P_{12} &= \dot{x}_1(x_1^*, y_1^*, x_2^*, y_2^*, y_3^*, \tau^*)\\ &= \sum_{j=1}^{2} \psi_{1j}\Big\{e^{-\eta_j t}\big[(-\eta_j a_j + \omega_{dj} b_j)\cos\omega_{dj} t\\ &\quad - (\omega_{dj} a_j + \eta_j b_j)\sin\omega_{dj} t\big]\\ &\quad + A_j\omega\cos(\omega t + \tau^*) - B_j\omega\sin(\omega t + \tau^*)\Big\},\end{aligned} \tag{15.2}$$

$$\begin{aligned}P_{13} &= x_2(x_1^*, y_1^*, x_2^*, y_2^*, y_3^*, \tau^*)\\ &= \sum_{j=1}^{2} \psi_{2j}\big[e^{-\eta_j t}(a_j\cos\omega_{dj} t + b_j\sin\omega_{dj} t)\\ &\quad + A_j\sin(\omega t + \tau^*) + B_j\cos(\omega t + \tau^*)\big],\end{aligned} \tag{15.3}$$

$$\begin{aligned}P_{14} &= \dot{x}_2(x_1^*, y_1^*, x_2^*, y_2^*, y_3^*, \tau^*)\\ &= \sum_{j=1}^{2} \psi_{2j}\Big\{e^{-\eta_j t}\big[(-\eta_j a_j + \omega_{dj} b_j)\cos\omega_{dj} t\\ &\quad - (\omega_{dj} a_j + \eta_j b_j)\sin\omega_{dj} t\big]\\ &\quad + A_j\omega\cos(\omega t + \tau^*) - B_j\omega\sin(\omega t + \tau^*)\Big\},\end{aligned} \tag{15.4}$$

$$\begin{aligned}P_{15} &= \dot{x}_3(x_1^*, y_1^*, x_2^*, y_2^*, y_3^*, \tau^*)\\ &= e^{-\eta_3 t}\big[(-\eta_3 a_3 + \omega_{d3} b_3)\cos\omega_{d3} t\\ &\quad - (\omega_{d3} a_3 + \eta_3 b_3)\sin\omega_{d3} t\big]\\ &\quad + A_3\omega\cos(\omega t + \tau^*) - B_3\omega\sin(\omega t + \tau^*),\end{aligned} \tag{15.5}$$

$$P_{16} = \omega t + \tau^*. \tag{15.6}$$

In (15.1)–(15.6), t is the duration from the moment impacting at the left stop to that impacting at the right stop. The time t is the function of initial conditions, and is determined by the equation $x_2^* - x_3^* = -h$ implicitly, which is the condition of impacting at the right stop. Then we have

$$\begin{aligned}&G(t, y_1^*, x_2^*, y_2^*, x_3^*, y_3^*, \tau^*)\\ &\quad = x_2(t) - x_3(t) + h\\ &\quad = \sum_{j=1}^{2} \psi_{2j}\big[e^{-\eta_j t}(a_j\cos\omega_{dj} t + b_j\sin\omega_{dj} t)\\ &\qquad + A_j\sin(\omega t + \tau^*) + B_j\cos(\omega t + \tau^*)\big]\\ &\qquad - \big[e^{-\eta_3 t}(a_3\cos\omega_{d3} t + b_3\sin(\omega_{d3} t)\\ &\qquad + A_3\sin(\omega t + \tau^*) + B_3\cos(\omega t + \tau^*)\big] + h\\ &\quad = 0.\end{aligned} \tag{16}$$

According to (16), we obtain $\frac{\partial t}{\partial x_1^*}$, $\frac{\partial t}{\partial y_1^*}$, $\frac{\partial t}{\partial x_2^*}$, $\frac{\partial t}{\partial y_2^*}$, $\frac{\partial t}{\partial y_3^*}$, $\frac{\partial t}{\partial \tau^*}$ by the implicit function theorem.

According to (13.1)–(13.6), (15.1)–(15.6), and (16), a_{ij}can be computed as follows by the chain rule; see Appendix. Subsequently, $D\mathbf{P}_3$ is obtained by the similar way. Therefore, the Jacobi matrix of the Poincaré map $\mathbf{P}$ can be computed as $D\mathbf{P} = D\mathbf{P}_4 \circ D\mathbf{P}_3 \circ D\mathbf{P}_2 \circ D\mathbf{P}_1$.

4 Computing the Lyapunov exponents and Lyapunov dimension based on the Poincaré map

Let $\mathbf{T_P}(\mathbf{x}^*) = \mathbf{D}_{\mathbf{X}^*}\mathbf{P}$ denoting the Jacobi matrix of the Poincaré map $\mathbf{P}$ at the initial map point $\mathbf{x}^*$, then

$$\mathbf{T}_\mathbf{P}^N(\mathbf{x}^*) = \mathbf{T_P}\big(\mathbf{P}^{N-1}\mathbf{x}^*\big)\cdots\mathbf{T_P}(\mathbf{P}\mathbf{x}^*)\mathbf{T_P}(\mathbf{x}^*) \tag{17}$$

where $\mathbf{P}^k\mathbf{x}^*$ represent the kth iteration of $\mathbf{P}$ at the point $\mathbf{x}^*$. Let Λ_j^N be eigenvalues of the matrix $\mathbf{T}_\mathbf{P}^N(\mathbf{x}^*)$, the Lyapunov exponents can be computed as [6]

$$\lambda_j = \lim_{N\to\infty}\frac{1}{N}\ln\big|\Lambda_j^N\big|, \quad j = 1, 2, 3, 4, 5, 6. \tag{18}$$

However, (18) cannot be used to calculate the Lyapunov exponents directly. The reason for this is that when the number of iteration of the map $\mathbf{P}$ increases, the components of matrix $\mathbf{T}_\mathbf{P}^N(\mathbf{x}^*)$ may become infinite for chaotic attractors and null for periodic attractors. To avoid the overflow trouble, the QR method, as a tool of continuous orthogonalization, is applied repeatedly to the computation [6, 7]. We are interested in the matrix product $\mathbf{T}_\mathbf{P}^N(\mathbf{x}^*)$. First, $\mathbf{T_P}(\mathbf{x}^*)$ is decomposed as

$$\mathbf{T_P}(\mathbf{x}^*) = \mathbf{Q}_1\mathbf{R}_1, \tag{19}$$

where $\mathbf{Q}_1$ is an orthogonal matrix and $\mathbf{R}_1$ is upper triangular with non-negative diagonal elements. If $\mathbf{T_P}(\mathbf{x}^*)$ is invertible, this decomposition is unique. Now let

$$\mathbf{T}_s^k = \mathbf{T_P}\big(\mathbf{P}^{k-1}\mathbf{x}^*\big)\mathbf{Q}_{k-1}, \quad k = 2, 3, \ldots, N. \tag{20}$$

If $\mathbf{T}_s^k$ is decomposed as

$$\mathbf{T}_s^k = \mathbf{Q}_k\mathbf{R}_k, \tag{21}$$

where Gram–Schmidt orthogonalization method is used to the decomposition, and $\mathbf{Q}_k$ is orthogonal and $\mathbf{R}_k$ is upper triangular with non-negative diagonal elements, then we have

$$\mathbf{T_P}\big(\mathbf{P}^{k-1}\mathbf{x}^*\big) = \mathbf{Q}_k\mathbf{R}_k\mathbf{Q}_{k-1}^{-1}. \tag{22}$$

According to (19) and (22), we obtain

$$\mathbf{T}_\mathbf{P}^N = \mathbf{Q}_N\mathbf{R}_N\mathbf{R}_{N-1}\cdots\mathbf{R}_1. \tag{23}$$

Let λ_{ii}^k be diagonal elements of the upper triangular matrix $\mathbf{R}_k$, and λ_{ii}^N be diagonal elements of the upper triangular matrix product $\mathbf{R}_N R_{N-1} \cdots \mathbf{R}_1$, we have

$$\lambda_{ii}^N = \prod_{k=1}^{N} \lambda_{ii}^k, \tag{24}$$

and the Lyapunov exponents can be computed as [6, 7]

$$\lambda_i = \lim_{N\to\infty} \frac{1}{N} \ln \lambda_{ii}^N, \tag{25}$$

where the Lyapunov exponents are ranked from large to small as

$$\lambda_1 \geq \lambda_2 \geq \cdots \geq \lambda_6. \tag{26}$$

Let K be the largest integer such that $\lambda_1 + \cdots + \lambda_K \geq 0$, the Lyapunov dimension as defined by Kaplan and York [14] is

$$D_L = K + \frac{\sum_{i=1}^{K} \lambda_i}{|\lambda_{K+1}|}, \tag{27}$$

where

$$\sum_{i=1}^{K} \lambda_i \geq 0, \quad \sum_{i=1}^{K+1} \lambda_i < 0. \tag{28}$$

If no such K exists, as is the case for a fixed point, D_L is defined to be 0.

5 Numerical analysis

5.1 Attractors, Lyapunov exponents, and Lyapunov dimension

The vibro-impact system with system parameters: $n = 1, \zeta = 0.0008, \zeta_p = 0.0009, R = 0.8, h = 0.05, u_{m1} = 0.8, u_{m2} = 1.5, u_{m3} = 1.0, u_{k1} = 0.8, u_{k2} = 0.9, u_{k3} = 1.0, u_{f1} = 1, u_{f2} = 0.6, u_{f3} = 1.0$, has been chosen for analysis, and the forcing frequency ω is taken as a control parameter. The Lyapunov exponents and Lyapunov dimension are computed, and are shown in the Table 1. The corresponding attractors shown in the projected Poincaré section (x_2, y_2) are represented in Fig. 2. With $\omega = 2.6790$ and 2.6715, the largest Lyapunov exponents equal to zero, indicating that the attractors of the Poincaré map are quasi-periodic, as shown in Fig. 2(a) and (d), respectively. With $\omega = 2.6770$ and 2.6760, the largest Lyapunov exponents are negative, indicating that the attractors of the Poincaré map are periodic, as shown in Fig. 2(b) and (c), respectively. Figure 2(b) exhibits period 5-5 fixed points, and Fig. 2(c) exhibits period 10-10 fixed points. With $\omega = 2.6660$ and 2.6620, the largest Lyapunov exponents are positive, indicating that the attractors of the Poincaré map are chaotic, as shown in Fig. 2(e) and (f), respectively. With $\omega = 2.6790$ and 2.6715, the Lyapunov dimensions are 1, implying that the projected Poincaré section exhibits a one-torus in the two cases.

With $\omega = 2.6760$, 2.6715, and 2.6620, the convergent series of the Lyapunov exponents are represented in Fig. 3. The iteration times (N) of the Poincaré map is 30,000. It is shown that for the periodic attractors and quasi-periodic attractors, the convergency of the Lyapunov exponents is good; see Fig. 3(a), (b) (the convergent series of the periodic attractor) and Fig. 3(c), (d) (the convergent series of the quasi-periodic attractor). However, for the chaotic attractor, the curves of the convergency series of the Lyapunov exponents is rough obviously, implying the convergency of the Lyapunov exponents of the chaotic attractor is not so good; see Fig. 3(e) and (f).

Table 1 The Lyapunov exponents, Lyapunov dimension, and the type of attractors of the Poincaré map

ω	Fig. name	λ_1	λ_2	λ_3	λ_4	λ_5	λ_6	Attractor	D_L
2.6790	2(a)	**0.0000**	−0.0059	−0.0356	−0.0356	−0.2328	−0.6014	Quasi-periodic	1
2.6770	2(b)	−0.0043	−0.0160	−0.0175	−0.0278	−0.0429	−0.8019	Periodic	0
2.6760	2(c)	−0.0043	−0.0058	−0.0247	−0.0252	−0.0415	−0.8088	Periodic	0
2.6715	2(d)	**0.0000**	−0.0032	−0.0242	−0.0243	−0.0660	−0.7929	Quasi-periodic	1
2.6660	2(e)	0.0158	**0.0000**	−0.0225	−0.0259	−0.0654	−0.8046	Chaotic	2.7022
2.6620	2(f)	0.0375	**0.0000**	−0.0218	−0.0263	−0.0713	−0.8219	Chaotic	3.5970

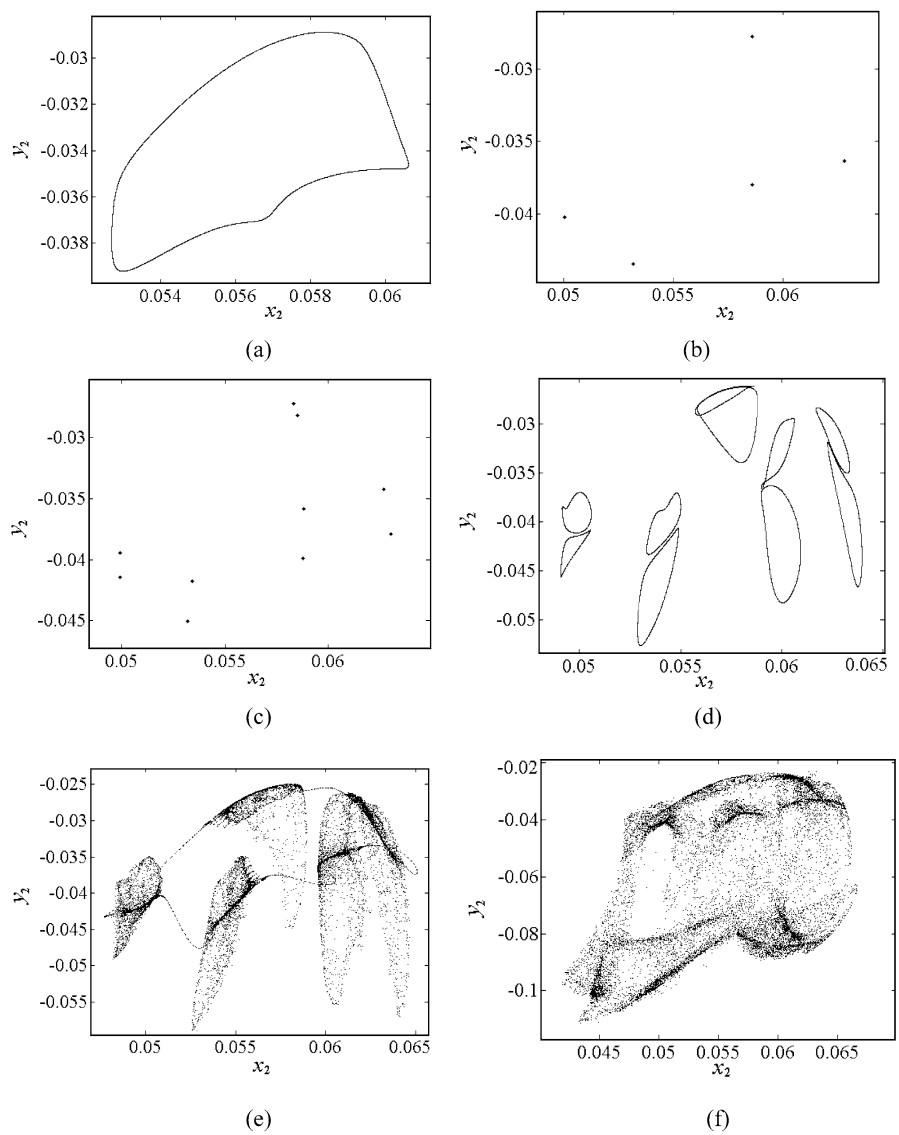

Fig. 2 Attractors shown in the projected Poincaré section (x_2, y_2). (**a**) $\omega = 2.6790$: quasi-periodic, (**b**) $\omega = 2.6770$: periodic, (**c**) $\omega = 2.6760$: periodic, (**d**) $\omega = 2.6715$: quasi-periodic, (**e**) $\omega = 2.6660$: chaotic, (**f**) $\omega = 2.6620$: chaotic

5.2 Characterizing quasi-periodic attractors by the Lyapunov dimension

Because of the complexity of the dynamics, the multi-degree-of-freedom vibro-impact system can exhibit complex quasi-periodic attractors, and approach chaos subsequently [24–29]. Here, we can characterize the various quasi-periodic attractors in vibro-impact systems by the Lyapunov dimension.

As an example, the system parameters (2): $n = 1$, $\varsigma = 0.015$, $\zeta_p = 0.005$, $\omega = 2.842$, $R = 0.8$, $h = 0.09$, $u_{m1} = 0.9$, $u_{m2} = 3$, $u_{m3} = 1.0$, $u_{k1} = 0.9$, $u_{k2} = 1.25$, $u_{k3} = 1.0$, $u_{f1} = 1.2$, $u_{f2} = 1.8$, $u_{f3} = 1.0$, is considered. When the iterating times increase successively, the projected Poincaré section will approach two different quasi-periodic attractors in turn. When the iterating times is 50,000, the projected Poincaré section approaches a circle, as shown in Fig. 4(a). However, when the iterating times increases, the circle becomes unstable, and converges upon a torus at last, as shown in Fig. 4(b). Figure 4(c) plots the last 50,000 map point after 200,000 iterates.

As another example, the vibro-impact system with system parameters (3): $n = 1$, $\zeta = 0.0016582$, $\zeta_p = 0.008$, $\omega = 3.88$, $R = 0.8$, $h = 0.08$, $u_{m1} = 0.76764$, $u_{m2} = 2$, $u_{m3} = 1.0$, $u_{k1} = 1$, $u_{k2} = 1$, $u_{k3} = 1.0$,

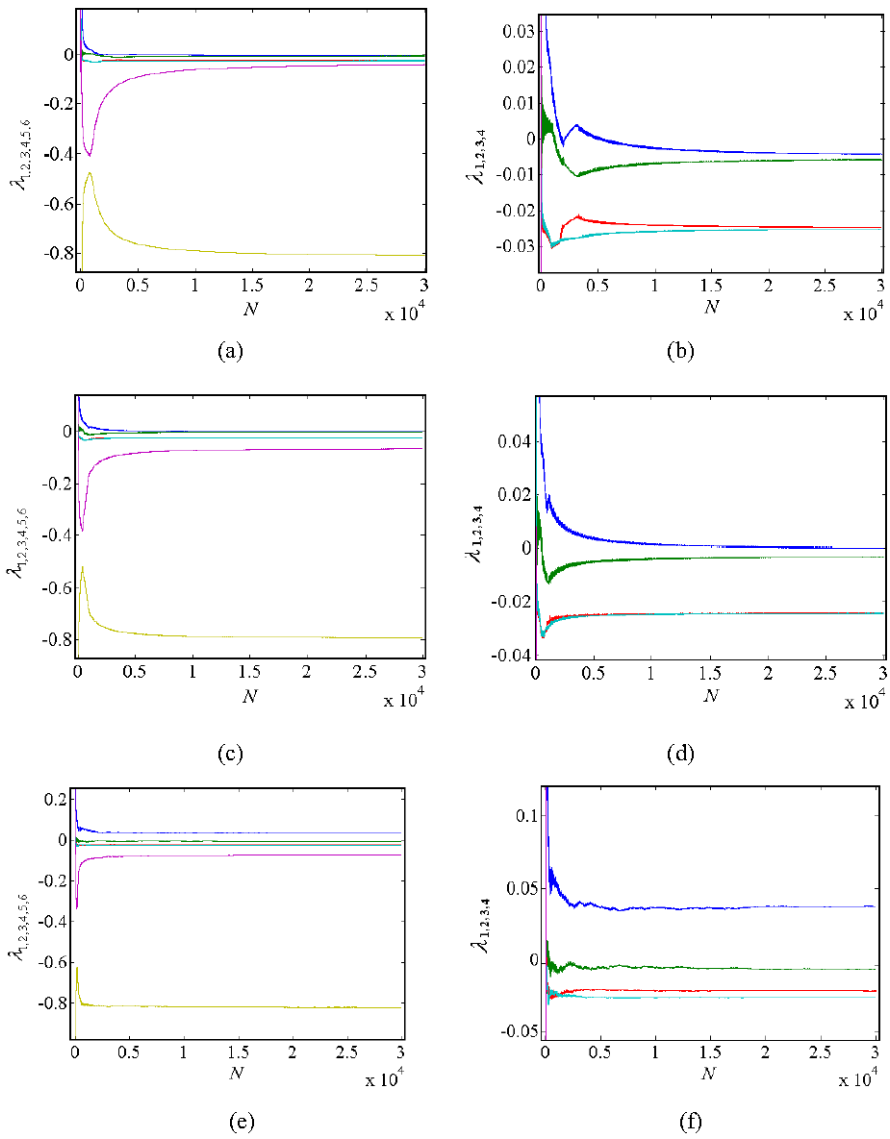

Fig. 3 The convergent series. (**a**) and (**b**) The convergent series of all the Lyapunov exponents with $\omega = 2.6760$, (**c**) and (**d**) The convergent series of all the Lyapunov exponents with $\omega = 2.6715$, (**e**) and (**f**) The convergent series of all the Lyapunov exponents with $\omega = 2.6620$

Table 2 The Lyapunov exponents, Lyapunov dimension, and the type of attractors of the Poincaré map

Fig. name	λ_1	λ_2	λ_3	λ_4	λ_5	λ_6	Attractor	D_L
4(c)	**0.0000**	**0.0000**	−0.0007	−0.0016	−0.5017	−0.5017	two-torus	2
5	**0.0000**	**0.0000**	**0.0000**	**0.0000**	−0.5008	−0.5008	four-torus	4

$u_{f1} = 2$, $u_{f2} = 1$, $u_{f3} = 1.0$, is considered. The projected Poincaré section exhibits a torus, as shown in Fig. 5.

The Lyapunov exponents and the Lyapunov dimension are computed as the Table 2. For the two cases, the largest Lyapunov exponents are all equal to zero, indicating that the attractors shown in the projected Poincaré section are quasi-periodic. For the attractor shown in Fig. 4(c), there are two zero Lyapunov exponents, hence the Lyapunov dimension is 2, indicating that the torus shown in Fig. 4(c) is a two-torus. However, for the attractor shown in Fig. 5, there are four

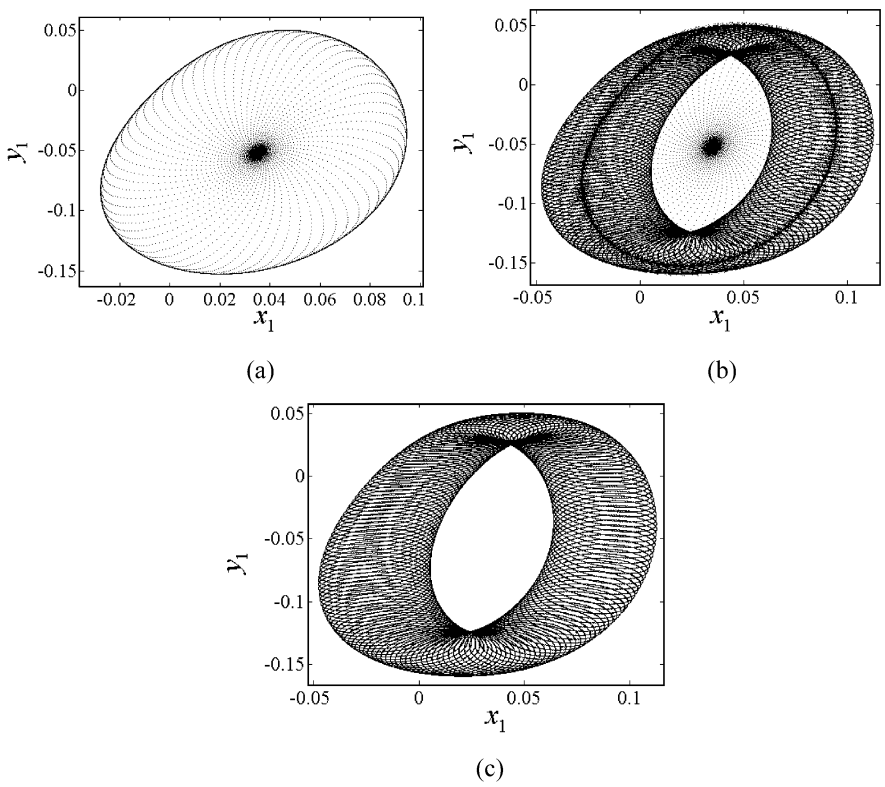

Fig. 4 Attractor shown in the projected Poincaré section (x_1, y_1); (**a**) iterate 50,000 times, (**b**) iterate 200,000 times, (**c**) plot the last 50,000 map point after 200,000 iterates

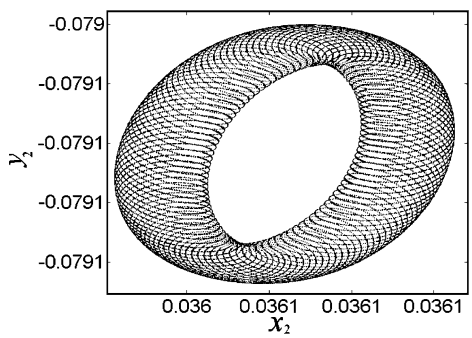

Fig. 5 Attractor shown in the projected Poincaré section (x_2, y_2)

zero Lyapunov exponents, hence the Lyapunov dimension is 4, indicating that the torus shown in Fig. 5 is a four-torus.

For the first case, the convergent series of $\lambda_{1,2,3,4}$ and $\lambda_{5,6}$ are shown in Fig. 6(a) and (b), respectively. The convergent series exhibit remarkable non-smooth characteristics before 50,000 iterates; this is because that the Poincaré section of the vibro-impact system approaches a unstable one-torus at first, as shown in Fig. 4(a). However, with the increasing of the iterate times, this final attractor is a two-torus, as shown in Fig. 4(c).

6 Conclusions

For the vibro-impact system, the Poincaré section can be chosen at the moment after impacting, and the six-dimensional Poincaré map can be established. The time between two consecutive impacts is determined by the initial conditions and the impact condition, hence the Poincaré map is an implicit map. The Poincaré map can be used to determine all the Lyapunov exponents and the Lyapunov dimension. By numerical simulations, the attractors are represented in the projected Poincaré section, and the Lyapunov spectrum is obtained. The multi-degree-of-freedom vibro-impact system may exhibit various complex quasi-periodic attractors, which can be classified by the Lyapunov dimension. The method for computing the Lyapunov exponents and the Lyapunov dimension is effective for both symmetric and unsymmetric vibro-impact systems.

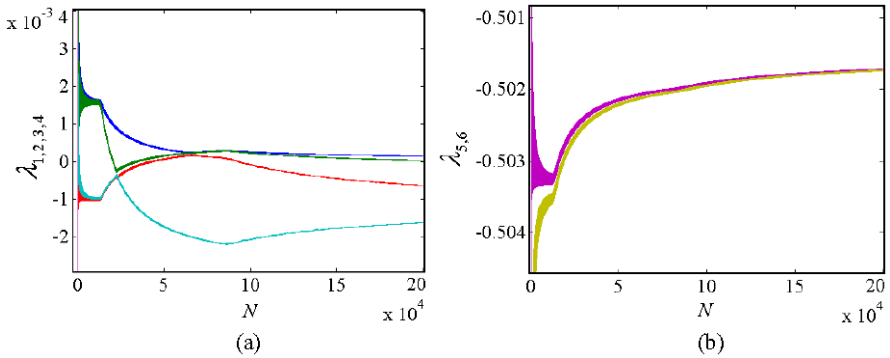

Fig. 6 The convergent series of the Lyapunov exponents with the second system parameters: (**a**) $\lambda_{1,2,3,4}$, (**b**) $\lambda_{5,6}$

Acknowledgements This work is supported by National Natural Science Foundation of China (10902092, 11172246, 11102030) and Fundamental Research Funds for the Central Universities of China (2009QK39) and Opening Fund of State Key Laboratory of Traction Power, Southwest Jiaotong University, China (Grant No. TPL1106).

Appendix

Jacobi matrix elements

$$a_{i1} = \frac{\partial P_{1i}}{\partial a_1}\frac{\partial a_1}{\partial x_1^*} + \frac{\partial P_{1i}}{\partial b_1}\frac{\partial b_1}{\partial x_1^*} + \frac{\partial P_{1i}}{\partial a_2}\frac{\partial a_2}{\partial x_1^*} + \frac{\partial P_{1i}}{\partial b_2}\frac{\partial b_2}{\partial x_1^*} + \frac{\partial P_{1i}}{\partial a_3}\frac{\partial a_3}{\partial x_1^*} + \frac{\partial P_{1i}}{\partial b_3}\frac{\partial b_3}{\partial x_1^*} + \frac{\partial P_{1i}}{\partial t}\frac{\partial t}{\partial x_1^*},$$

$$a_{i2} = \frac{\partial P_{1i}}{\partial a_1}\frac{\partial a_1}{\partial y_1^*} + \frac{\partial P_{1i}}{\partial b_1}\frac{\partial b_1}{\partial y_1^*} + \frac{\partial P_{1i}}{\partial a_2}\frac{\partial a_2}{\partial y_1^*} + \frac{\partial P_{1i}}{\partial b_2}\frac{\partial b_2}{\partial y_1^*} + \frac{\partial P_{1i}}{\partial a_3}\frac{\partial a_3}{\partial y_1^*} + \frac{\partial P_{1i}}{\partial b_3}\frac{\partial b_3}{\partial y_1^*} + \frac{\partial P_{1i}}{\partial t}\frac{\partial t}{\partial y_1^*},$$

$$a_{i3} = \frac{\partial P_{1i}}{\partial a_1}\frac{\partial a_1}{\partial x_2^*} + \frac{\partial P_{1i}}{\partial b_1}\frac{\partial b_1}{\partial x_2^*} + \frac{\partial P_{1i}}{\partial a_2}\frac{\partial a_2}{\partial x_2^*} + \frac{\partial P_{1i}}{\partial b_2}\frac{\partial b_2}{\partial x_2^*} + \frac{\partial P_{1i}}{\partial a_3}\frac{\partial a_3}{\partial x_2^*} + \frac{\partial P_{1i}}{\partial b_3}\frac{\partial b_3}{\partial x_2^*} + \frac{\partial P_{1i}}{\partial t}\frac{\partial t}{\partial x_2^*},$$

$$a_{i4} = \frac{\partial P_{1i}}{\partial a_1}\frac{\partial a_1}{\partial y_2^*} + \frac{\partial P_{1i}}{\partial b_1}\frac{\partial b_1}{\partial y_2^*} + \frac{\partial P_{1i}}{\partial a_2}\frac{\partial a_2}{\partial y_2^*} + \frac{\partial P_{1i}}{\partial b_2}\frac{\partial b_2}{\partial y_2^*} + \frac{\partial P_{1i}}{\partial a_3}\frac{\partial a_3}{\partial y_2^*} + \frac{\partial P_{1i}}{\partial b_3}\frac{\partial b_3}{\partial y_2^*} + \frac{\partial P_{1i}}{\partial t}\frac{\partial t}{\partial y_2^*},$$

$$a_{i5} = \frac{\partial P_{1i}}{\partial a_1}\frac{\partial a_1}{\partial y_3^*} + \frac{\partial P_{1i}}{\partial b_1}\frac{\partial b_1}{\partial y_3^*} + \frac{\partial P_{1i}}{\partial a_2}\frac{\partial a_2}{\partial y_3^*} + \frac{\partial P_{1i}}{\partial b_2}\frac{\partial b_2}{\partial y_3^*} + \frac{\partial P_{1i}}{\partial a_3}\frac{\partial a_3}{\partial y_3^*} + \frac{\partial P_{1i}}{\partial b_3}\frac{\partial b_3}{\partial y_3^*} + \frac{\partial P_{1i}}{\partial t}\frac{\partial t}{\partial y_3^*},$$

$$a_{i6} = \frac{\partial P_{1i}}{\partial a_1}\frac{\partial a_1}{\partial \tau^*} + \frac{\partial P_{1i}}{\partial b_1}\frac{\partial b_1}{\partial \tau^*} + \frac{\partial P_{1i}}{\partial a_2}\frac{\partial a_2}{\partial \tau^*} + \frac{\partial P_{1i}}{\partial b_2}\frac{\partial b_2}{\partial \tau^*} + \frac{\partial P_{1i}}{\partial a_3}\frac{\partial a_3}{\partial \tau^*} + \frac{\partial P_{1i}}{\partial b_3}\frac{\partial b_3}{\partial \tau^*} + \frac{\partial P_{1i}}{\partial t}\frac{\partial t}{\partial \tau^*}.$$

References

1. Oseledec, V.I.: A multiplicative ergodic theorem: Lyapunov characteristic numbers for dynamical system. Trans. Mosc. Math. Soc. **19**, 197–231 (1968)
2. Guckenheimer, J., Holmes, P.: Nonlinear Oscillations, Dynamical System, and Bifurcations of Vector Fields. Springer, New York (1983)
3. Parker, T.S., Chua, L.O.: Practical Numerical Algorithms for Chaotic Systems. Springer, Berlin (1989)
4. Ott, E.: Chaos in Dynamic Systems. Cambridge University Press, New York (1993)
5. Wolf, A., Swift, J.B., Swinney, H.L., Vastano, J.A.: Determining Lyapunov exponents from a time series. Physica D **16**, 285–317 (1985)
6. Eckmann, J.-P., Ruelle, D.: Ergodic theory of chaos and strange attractors. Rev. Mod. Phys. **57**, 617–656 (1985)
7. Eckmann, J.-P., Kamphorst, S.O., Ruelle, D., Ciliberto, S.: Lyapunov exponents from time series. Phys. Rev. A **34**, 4971–4979 (1986)
8. Brown, R., Bryant, P., Abarbanel, H.D.I.: Computing the Lyapunov spectrum of a dynamical system from an observed time series. Phys. Rev. A **43**, 2787–2806 (1991)
9. Lu, J., Yang, G.L., Oh, H., Luo, A.C.J.: Computing Lyapunov exponents of continuous systems: methods of Lyapunov vectors. Chaos Solitons Fractals **23**, 1879–1892 (2005)
10. Yang, C.X., Wu, C.Q.: A robust method on estimation of Lyapunov exponents from a noisy time series. Nonlinear Dyn. **64**(3), 279–292 (2011)
11. Soriano, D.C., Fazanaro, R.S.R., de Oliveira, J.R., Attux, R., Madrid, M.K.: A method for Lyapunov spectrum estimation using cloned dynamics and its application to the discontinuously-excited FitzHugh-Nagumo model. Nonlinear Dyn. (2011). doi:10.1007/s11071-011-9989-2
12. Stefański, A., Kapitaniak, T.: Estimation of the dominant Lyapunov exponent of non-smooth systems on the basis of maps synchronization. Chaos Solitons Fractals **15**, 233–244 (2003)
13. Müller, P.C.: Calculation of Lyapunov exponents for dynamic systems with discontinuities. Chaos Solitons Fractals **5**(9), 1671–1681 (1995)

14. Stefański, A.: Estimation of the largest Lyapunov exponent in systems with impacts. Chaos Solitons Fractals **11**, 2443–2451 (2000)
15. de Souza, S.L.T., Caldas, I.L.: Calculation of Lyapunov exponents in systems with impacts. Chaos Solitons Fractals **19**, 569–579 (2004)
16. Janin, O., Lamarque, C.H.: Stability of singular periodic motions in a vibro-impact oscillator. Nonlinear Dyn. **28**(3–4), 231–241 (2002)
17. Jin, L., Lu, Q.S., Twizell, E.H.: A method for calculating the spectrum of Lyapunov exponents by local maps in non-smooth impact-vibrating systems. J. Sound Vib. **298**, 1019–1033 (2006)
18. Awrejcewicz, J., Kudra, G.: Stability analysis and Lyapunov exponents of a multi-body mechanical system with rigid unilateral constraints. Nonlinear Anal. **63**, 909–918 (2005)
19. Kaplan, J.L., Yorke, J.A.: Chaotic behavior of multidimensional difference equations. In: Lecture Notes in Mathematics, pp. 228–237. Springer, New York (1979)
20. Frederickson, P., Kaplan, J.L., Yorke, E.D., Yorke, J.A.: The Lyapunov dimension of strange attractors. J. Differ. Equ. **49**, 185–207 (1983)
21. Russell, D.A., Hanson, J.D., Ott, E.: Dimension of Strange attractors. Phys. Rev. Lett. **45**(14), 1175–1178 (1980)
22. Ledrappier, F.: Some relations between dimension and Lyapunov exponents. Commun. Math. Phys. **81**, 229–238 (1981)
23. Yue, Y., Xie, J.H.: Lyapunov exponents and coexistence of attractors in vibro-impact systems with symmetric two-sided constraints. Phys. Lett. A **373**, 2041–2046 (2009)
24. Luo, G.W., Xie, J.H.: Hopf bifurcation of a two-degree-of-freedom vibro-impact system. J. Sound Vib. **213**(3), 391–408 (1998)
25. Luo, G.W., Xie, J.H.: Bifurcation and chaos in a system with impacts. Physica D **148**, 183–200 (2001)
26. Luo, G.W., Xie, J.H.: Hopf bifurcation and chaos of a two-degree-of-freedom vibro-impact system in two strong resonance cases. Int. J. Non-Linear Mech. **37**(1), 19–34 (2002)
27. Xie, J.H., Ding, W.C.: Hopf-Hopf bifurcation and invariant torus T^2 of a vibro-impact system. Int. J. Non-Linear Mech. **40**, 531–543 (2005)
28. Ding, W.C., Xie, J.H.: Torus T^2 and its routes to chaos of a vibro-impact system. Phys. Lett. A **349**, 324–330 (2006)
29. Ding, W.C., Xie, J.H.: Dynamical analysis of a two-parameter family for a vibro-impact system in resonance cases. J. Sound Vib. **287**, 101–115 (2005)